Electronic Supplementary Information

Water-mediated exsolution of nanoparticles in alkali metal-doped perovskite structured triple-conducting oxygen catalysts for reversible cells

Kwangho Park[a, †], Muhammad Saqib[a, b, †], Hyungwoo Lee[c, †], Donghwi Shin[d], Minkyeong Jo[a], Kwang Min Park[a], Muhammad Hamayun[a], Seo Hyun Kim[a], Sungkyu Kim[a], Kug-Seung Lee[e], Ryan O'Hayre[f], Minseok Choi[c, *], Sun-Ju Song[d, *], Jun-Young Park[a, *]

[a] *HMC, Department of Nanotechnology and Advanced Materials Engineering, Sejong University, Seoul 05006, Korea*

[b] *Maryland Energy Innovation Institute, Department of Materials Science and Engineering, University of Maryland, College Park, MD 20742, United States*

[c] *Department of Physics, Inha University, Incheon 22212, Korea*

[d] *Department of Materials Science and Engineering, Chonnam National University, Gwangju 61186, Korea*

[e] *Pohang Accelerator Laboratory, Pohang 37673, Korea*

[f] *Department of Metallurgical and Materials Engineering, Colorado School of Mines, Golden, CO 80401, United States*

† These authors contributed equally to this work.

* Correspondence and requests for materials should be addressed to J.-Y. Park (email: jyoung@sejong.ac.kr), S.-J. Song (email: song@chonnam.ac.kr), and M. Choi (email: minseok.choi@inha.ac.kr).

Table S1 Crystal-structural parameters of cubic perovskite $A_{0.05}Ba_{0.95}Co_{0.4}Fe_{0.4}Zr_{0.1}Y_{0.1}O_{3-\delta}$ (A = Li, Na, and K) materials from Rietveld refinement.

Properties	**$A_{0.05}Ba_{0.95}Co_{0.4}Fe_{0.4}Zr_{0.1}Y_{0.1}O_{3-\delta}$**		
Alkali metal (A)	Li	Na	K
Phase structure (space group)	Cubic (*Pm-3m*)		
a, b, c (Å)	4.0980	4.1090	4.0946
V (Å^3)	68.834	69.376	68.647
R_p	3.21	3.01	3.21
R_{wp}	4.54	4.23	4.67
χ^2	1.81	1.61	2.12

Table S2 Crystal-structural parameters of cubic perovskite $K_xBa_{1-x}Co_{0.4}Fe_{0.4}Zr_{0.1}Y_{0.1}O_{3-\delta}$ (x = 0.25, 0.5, and 0.75) materials from Rietveld refinement.

Properties	**$K_xBa_{1-x}Co_{0.4}Fe_{0.4}Zr_{0.1}Y_{0.1}O_{3-\delta}$**		
Doping concentration (x)	2.5	5	7.5
Phase structure (space group)	Cubic (*Pm-3m*)		
a, b, c (Å)	4.1059	4.0946	4.0918
V (Å^3)	69.223	68.647	68.509
R_p	3.65	3.21	3.13
R_{wp}	4.77	4.67	4.26
χ^2	0.97	2.12	1.38

Table S3 Crystal-structural parameters of cubic perovskite $K_{0.05}Ba_{0.95}Co_{0.4}Fe_{0.4}Zr_{0.2-y}Y_yO_{3-\delta}$ (y = 0.25, 0.5, and 0.75) materials from Rietveld refinement.

Properties	**$K_{0.05}Ba_{0.95}Co_{0.4}Fe_{0.4}Zr_{0.2-y}Y_yO_{3-\delta}$**				
Doping concentration (y)	0.02	0.04	0.06	0.08	0.1
Phase structure (space group)	Cubic (*Pm-3m*)				
a, b, c (Å)	4.0860	4.0880	4.0890	4.0910	4.0946
V (Å^3)	68.212	68.339	68.403	68.468	68.647
R_p	3.21	3.05	3.08	3.09	3.21
R_{wp}	4.32	4.38	4.42	4.35	4.67
χ^2	1.34	1.86	1.79	1.87	2.12

Table S4 Weight change (hydration properties, ΔW) of BCFZY and KBCFZY materials depending on changes in pO_2 and pH_2O from the thermogravimetric analysis.

Materials	Temp. (°C)	W_T [1] (mg)	ΔW_D [2] (μg)	ΔW_W [3] (μg)	ΔW_H [4] (μg)	$\Delta W_H/\Delta W_T$ [5] (%)
BCFZY	700	256.472	–9.7±0.15	9.1±0.21	18.8±0.53	7.3±0.13
	650	256.607	–10.6±0.14	9.5±0.21	20.1±0.21	7.8±0.1
	600	256.763	–11.5±0.46	10.0±0.16	21.5±0.27	8.4±0.26
KBCFZY	700	300.287	–12.0±0.14	21.4±0.35	33.4±0.31	11.1±0.1
	650	300.428	–12.4±0.99	26.9±0.60	39.4±1.46	13.1±0.49
	600	300.586	–14.2±0.41	28.2±0.33	42.5±0.58	14.1±0.19

[1] W_T: Total sample weight at certain temperature.

[2] ΔW_D (W_D–W_T): Weight change for oxidation reaction (dry condition).

[3] ΔW_W (W_W–W_T): Weight change for hydration reaction (wet condition).

[4] ΔW_H (W_H–W_D): Weight change for hydration and hydrogenation reaction.

[5] $\Delta W_H/\Delta W_T$: Percentage of hydrogen solubility under hydrogenation reaction.

Table S5 Bader charge of the oxygen atom at eight distinguishable oxygen sites (See **Fig. S17**).

Bader charge (e)	BCFZY	KBCFZY
Co-O-Fe	–0.957	–0.881
Co-O-Co	–0.981	–0.983
Fe-O-Fe	–1.126	–1.065
Y-O-Co	–1.147	–1.106
Y-O-Fe	–1.225	–1.213
Zr-O-Co	–1.126	–1.233
Zr-O-Fe	–1.199	–1.194
Y-O-Zr	–1.351	–1.350

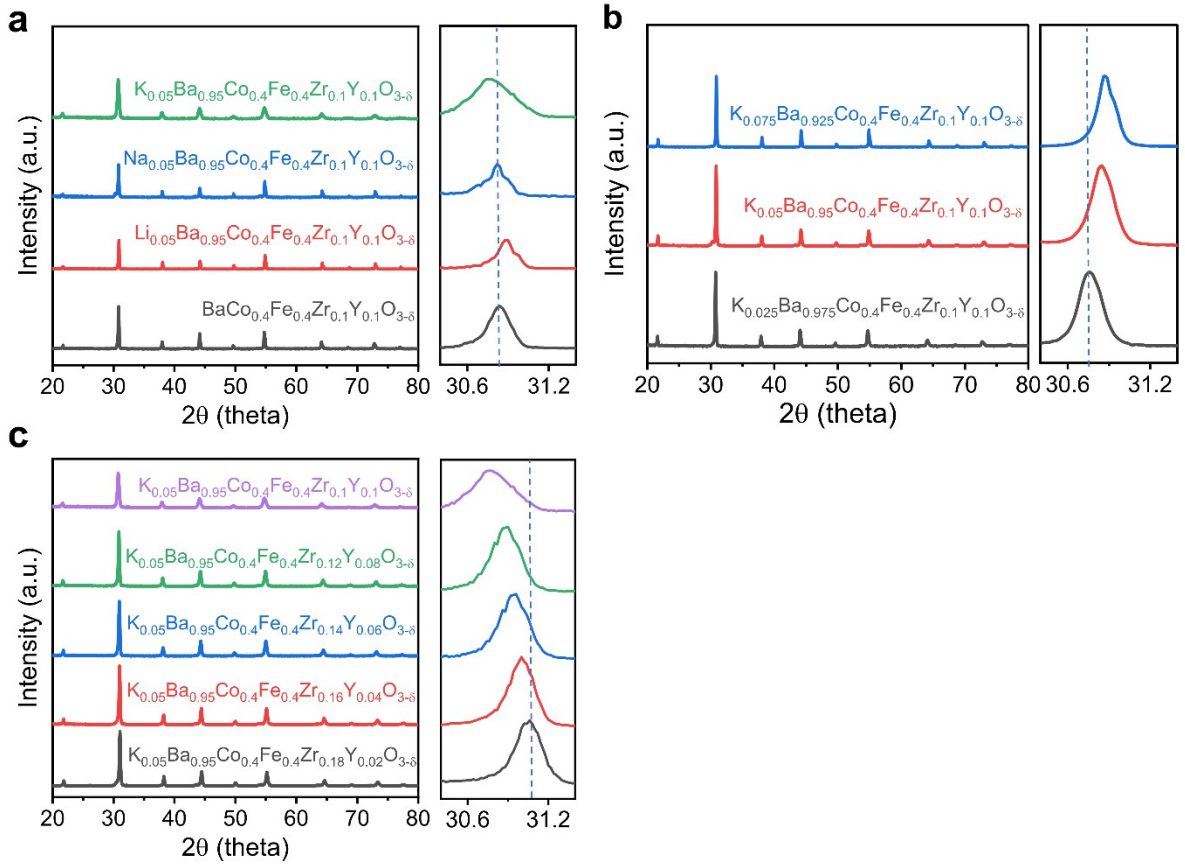

Fig. S1 Structure and phase purity analyses of BCFZY and $A_xBa_{1-x}Co_{0.4}Fe_{0.4}Zr_{0.2-y}Y_yO_{3-\delta}$ perovskite by XRD. (a) $A_{0.05}Ba_{0.95}Co_{0.4}Fe_{0.4}Zr_{0.1}Y_{0.1}O_{3-\delta}$ (A = Li, Na, and K). (b) $K_xBa_{1-x}Co_{0.4}Fe_{0.4}Zr_{0.1}Y_{0.1}O_{3-\delta}$ (x = 0.025, 0.5, 0.075). (c) $K_{0.05}Ba_{0.95}Co_{0.4}Fe_{0.4}Zr_{0.2-y}Y_yO_{3-\delta}$ (y = 0.02, 0.04, 0.06, 0.08 and 0.1).

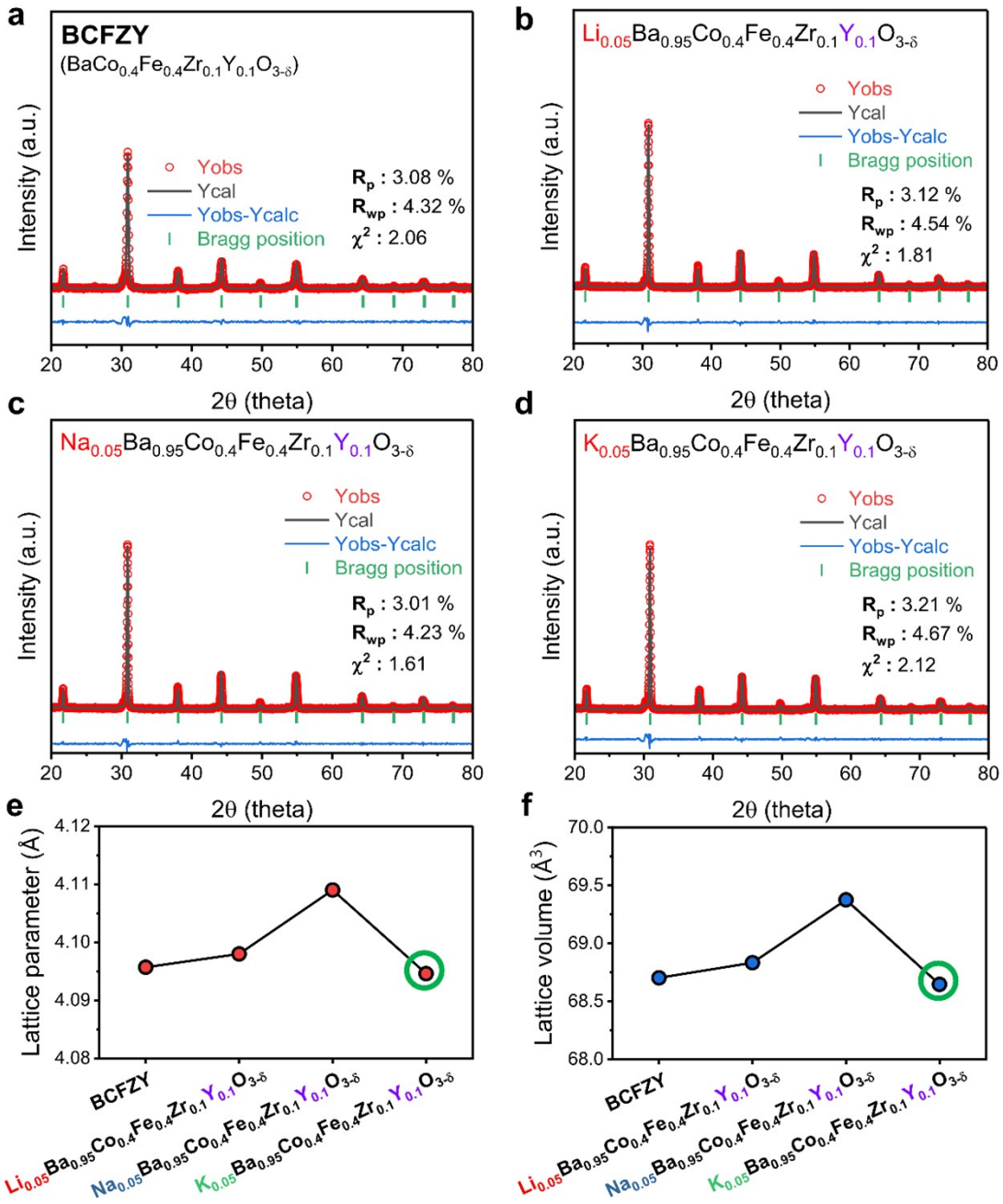

Fig. S2 Rietveld refinement results of the ABCFZY perovskites (varying alkali metal species). (a) BCFZY. (b) $\mathbf{Li_{0.05}}Ba_{0.95}Co_{0.4}Fe_{0.4}\mathbf{Zr_{0.1}Y_{0.1}}O_{3-\delta}$. (c) $\mathbf{Na_{0.05}}Ba_{0.95}Co_{0.4}Fe_{0.4}\mathbf{Zr_{0.1}Y_{0.1}}O_{3-\delta}$. (d) $\mathbf{K_{0.05}}Ba_{0.95}Co_{0.4}Fe_{0.4}\mathbf{Zr_{0.1}Y_{0.1}}O_{3-\delta}$. (e) Lattice parameters. (f) Lattice volumes.

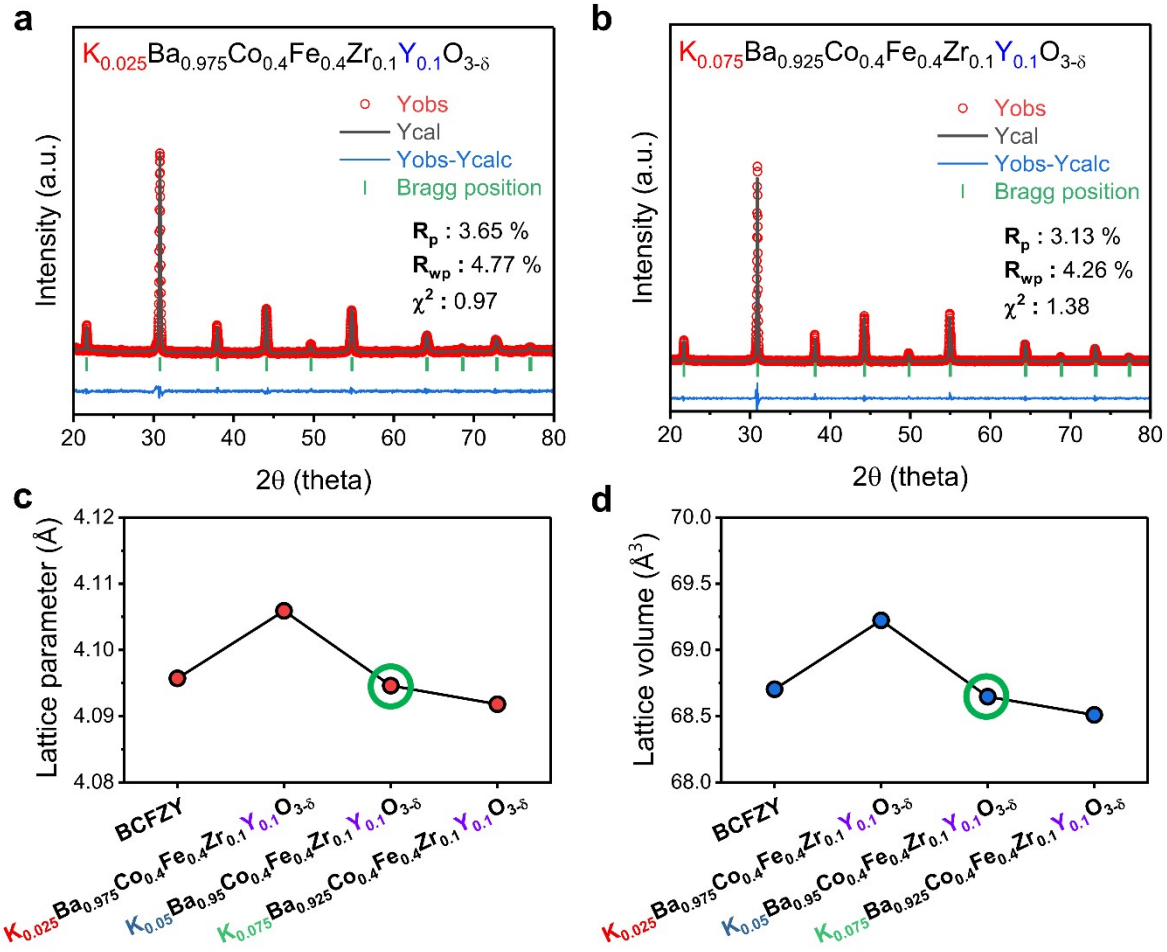

Fig. S3. Rietveld refinement results of the KBCFZY perovskite (varying K dopant concentration). (a) $\mathbf{K_{0.025}}Ba_{0.975}Co_{0.4}Fe_{0.4}Zr_{0.1}Y_{0.1}O_{3-\delta}$. (b) $\mathbf{K_{0.075}}Ba_{0.925}Co_{0.4}Fe_{0.4}Zr_{0.1}Y_{0.1}O_{3-\delta}$. (c) Lattice parameters. (d) Lattice volumes.

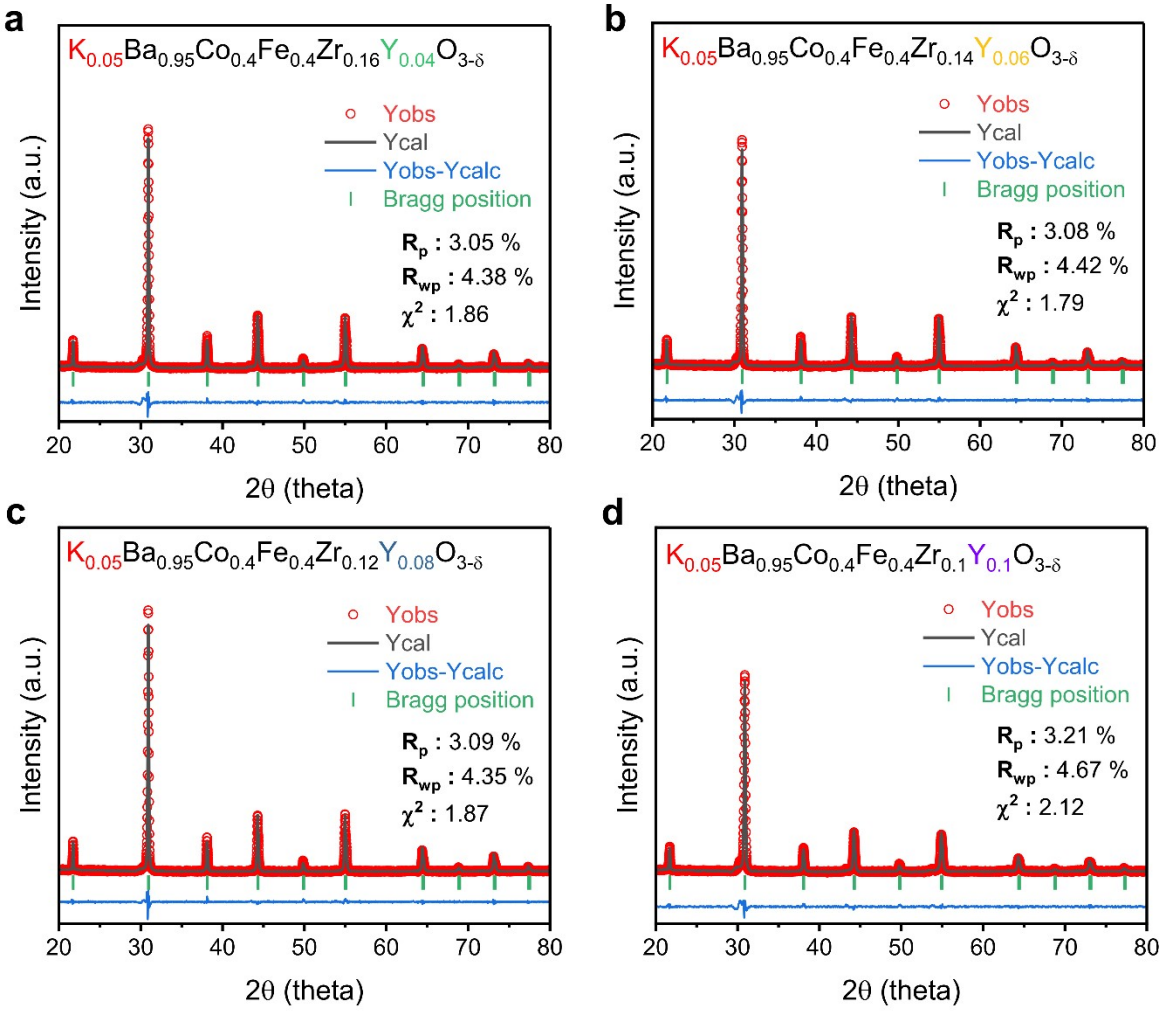

Fig. S4 Rietveld refinement results of the KBCFZY perovskite (varying Y dopant concentration). (a) $K_{0.05}Ba_{0.95}Co_{0.4}Fe_{0.4}\mathbf{Zr_{0.16}Y_{0.04}}O_{3-\delta}$. (b) $K_{0.05}Ba_{0.95}Co_{0.4}Fe_{0.4}\mathbf{Zr_{0.14}Y_{0.06}}O_{3-\delta}$. (c) $K_{0.05}Ba_{0.95}Co_{0.4}Fe_{0.4}\mathbf{Zr_{0.12}Y_{0.08}}O_{3-\delta}$. (d) $K_{0.05}Ba_{0.95}Co_{0.4}Fe_{0.4}\mathbf{Zr_{0.1}Y_{0.1}}O_{3-\delta}$.

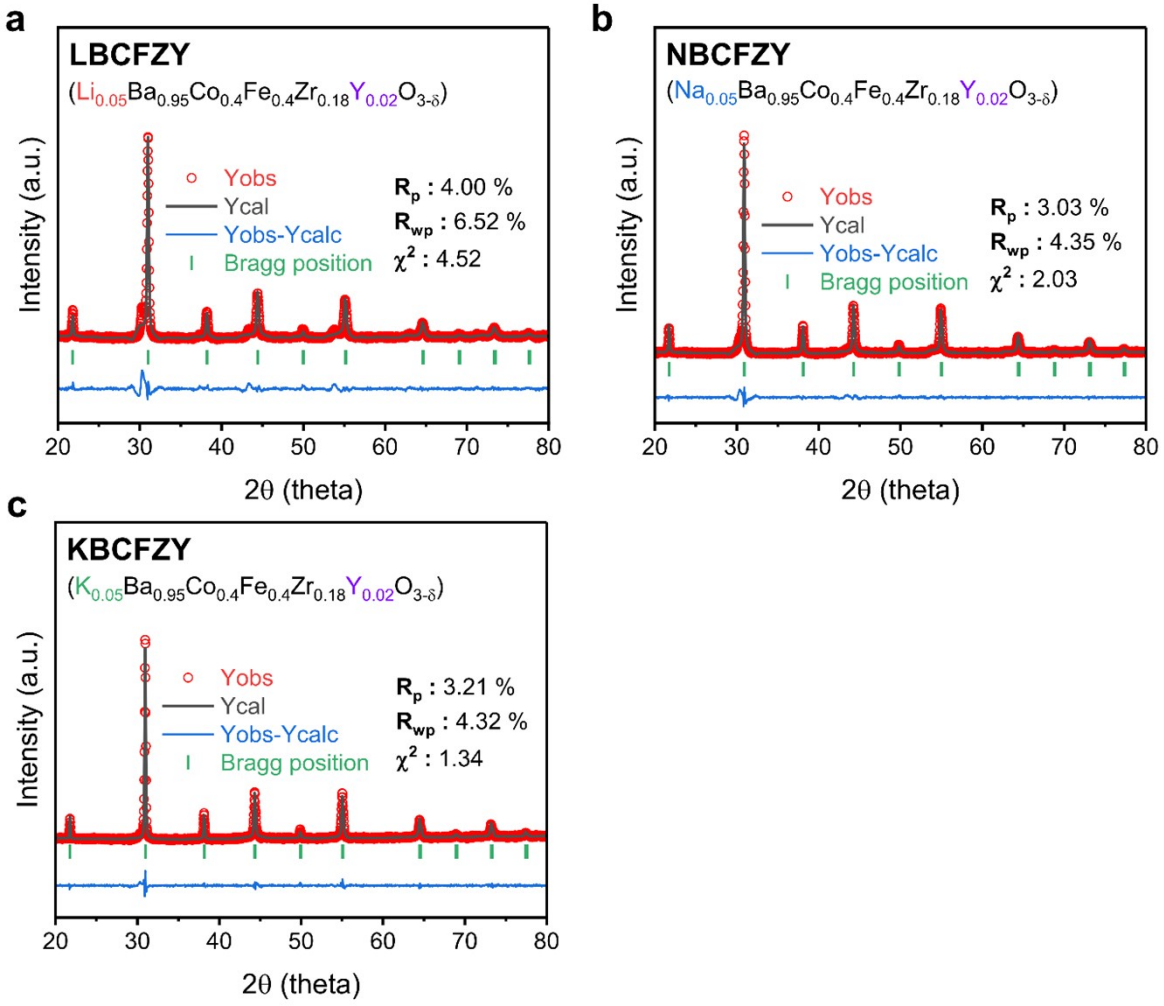

Fig. S5 Rietveld refinement results of the ABCFZY perovskites (varying alkali metal species). (a) $\mathbf{Li_{0.05}}Ba_{0.95}Co_{0.4}Fe_{0.4}\mathbf{Zr_{0.18}Y_{0.02}}O_{3-\delta}$ (LBCFZY). (b) $\mathbf{Na_{0.05}}Ba_{0.95}Co_{0.4}Fe_{0.4}\mathbf{Zr_{0.18}Y_{0.02}}O_{3-\delta}$ (NBCFZY). (c) $\mathbf{K_{0.05}}Ba_{0.95}Co_{0.4}Fe_{0.4}\mathbf{Zr_{0.18}Y_{0.02}}O_{3-\delta}$ (KBCFZY).

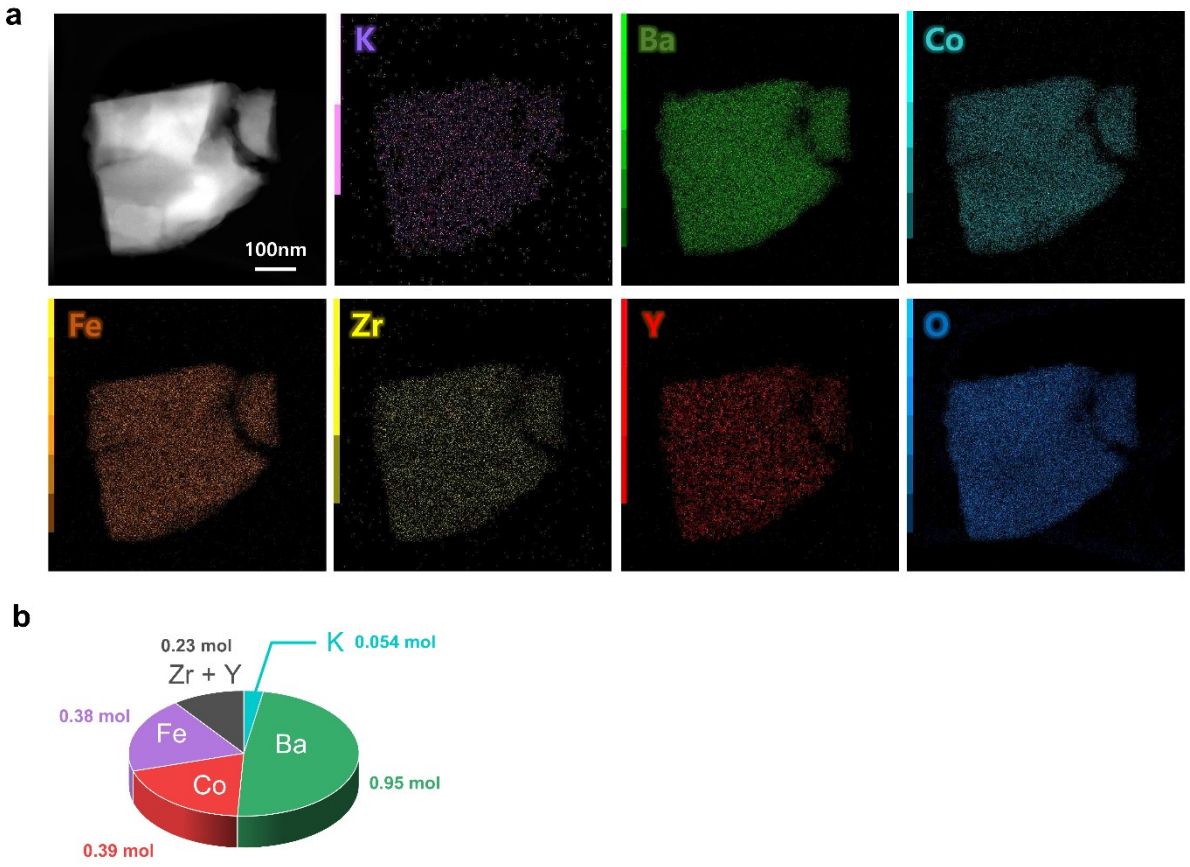

Fig. S6 KBCFZY composition analysis. (a) TEM-EDX elemental mapping results of KBCFZY. (b) ICP-OES analysis of BCFZY and KBCFZY.

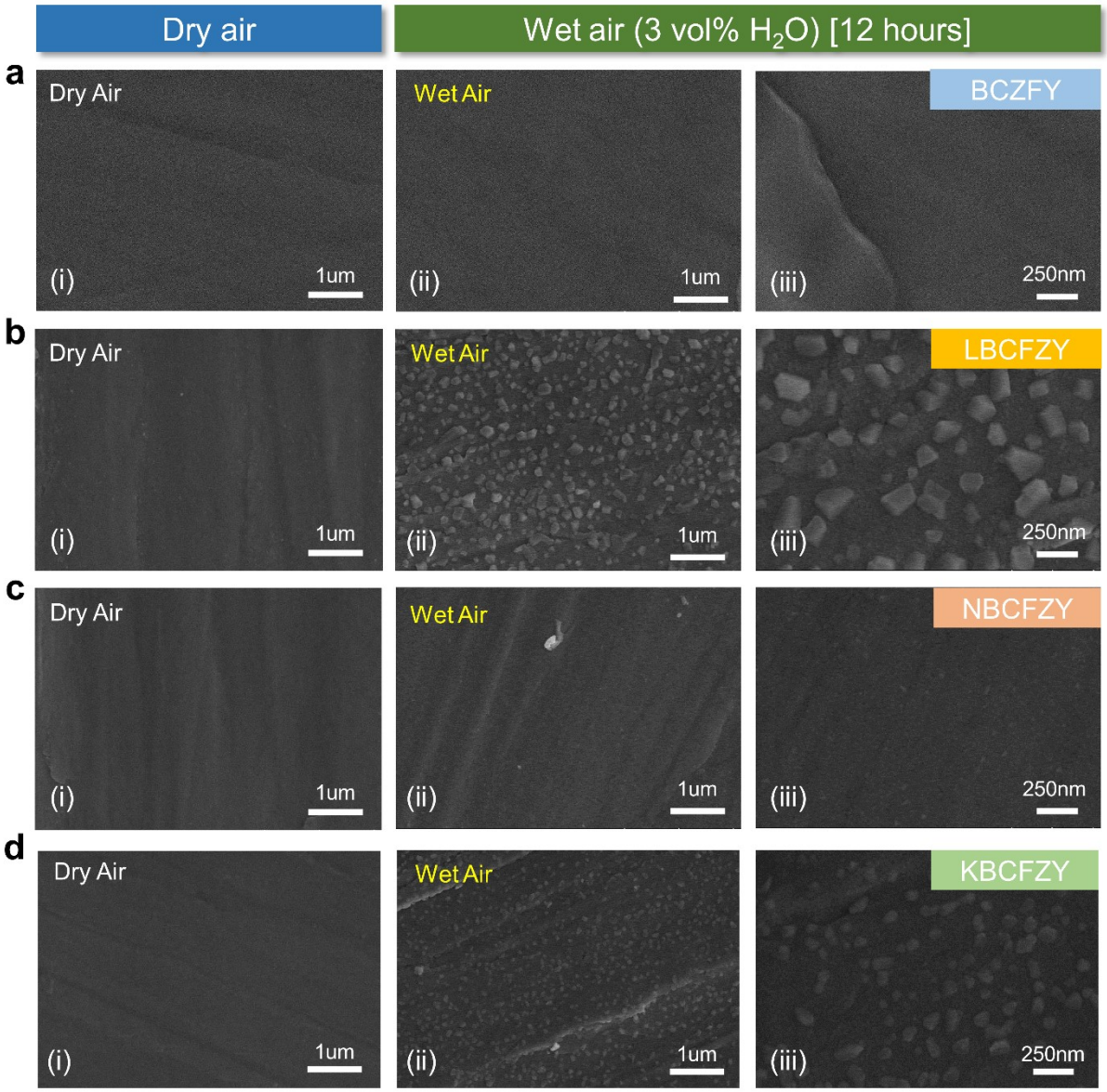

Fig. S7 FE-SEM images before and after exposure to humid (3 vol% H_2O) air for 12 hours at 600 ℃. (a) BCFZY. (b) LBCFZY. (c) NBCFZY. (d) KBCFZY.

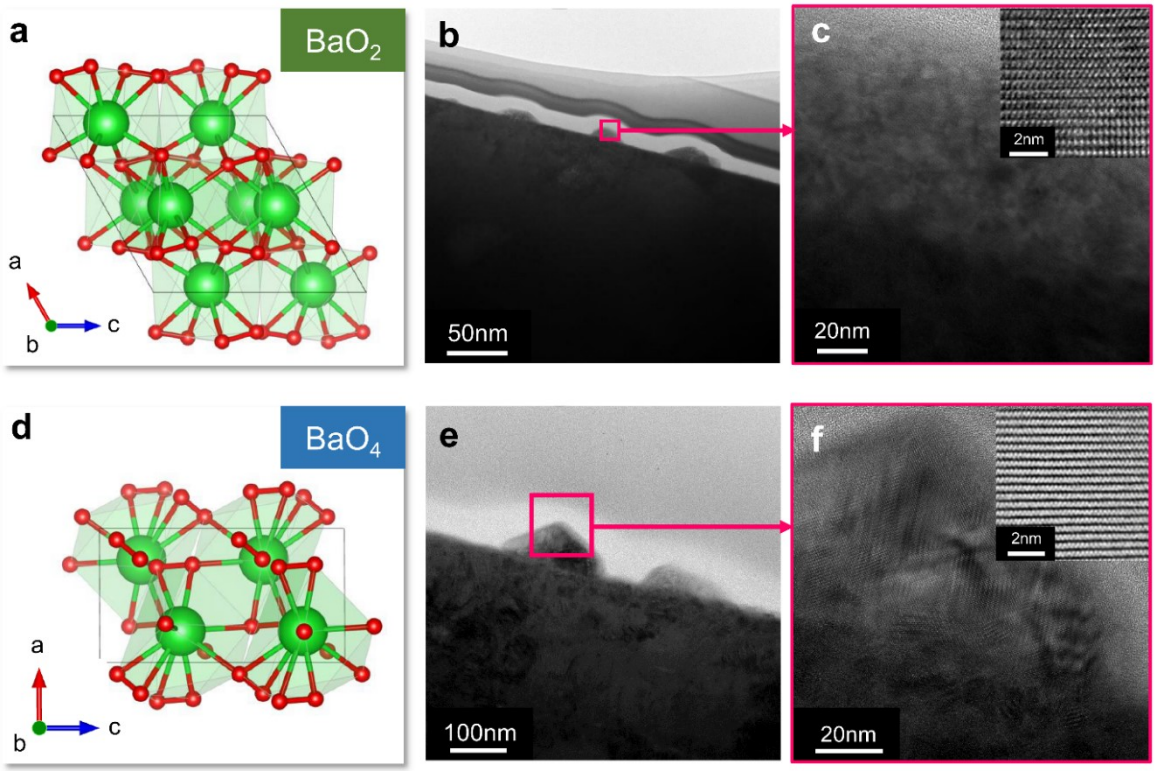

Fig. S8 Exsolution of catalytically active BaO_x nanocatalysts on ABCFZY perovskite oxide surfaces. (a) Scheme of BaO_2 crystalline structure. (b) TEM analysis of exsolved BaO_2 in LBCFZY. (c) HR-TEM image of exsolved BaO_2 (right inset: magnified HR-TEM image of BaO_2). (d) Scheme of BaO_4 crystalline structure. (e) TEM analysis of exsolved BaO_4 in KBCFZY. (f) HR-TEM image of exsolved BaO_4 (right inset: high-angle annular dark-field (HADDF)-STEM imaging of BaO_4).

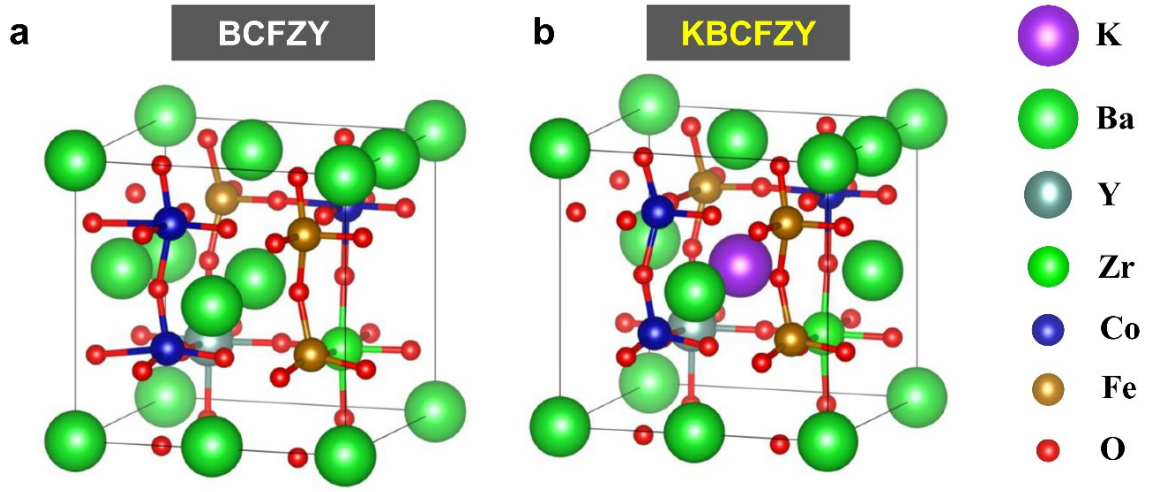

Fig. S9 Atomistic structures of BCFZY and KBCFZY obtained using DFT calculations. (a) BCFZY. (b) KBCFZY.

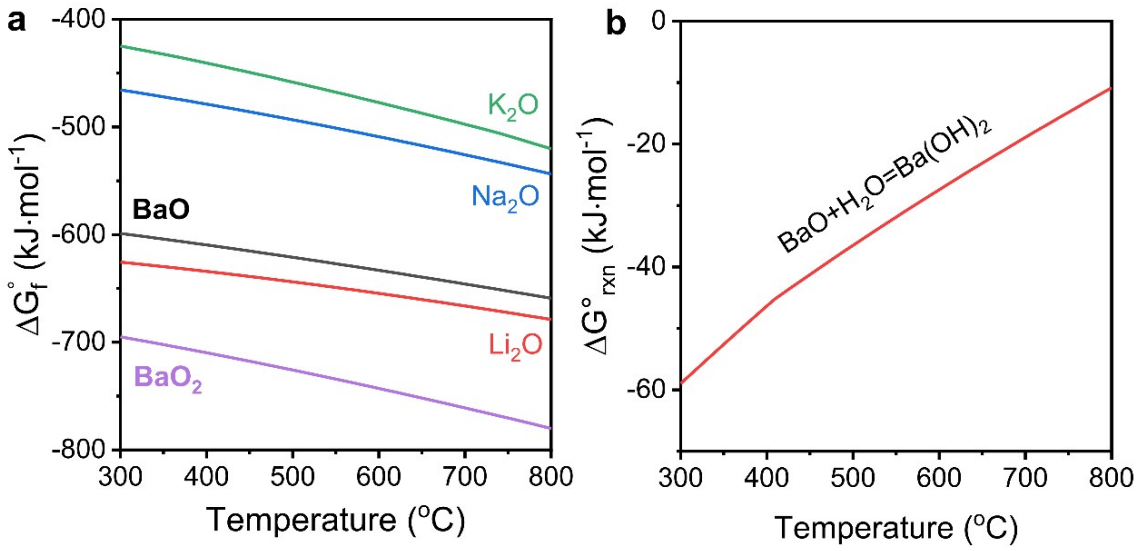

Fig. S10 Thermodynamic calculations of barium-related species as a function of pO_2, pH_2O, and temperature. (a) Gibbs free energy for the formation of BaO, BaO_2, Li_2O, Na_2O and K_2O phases. (b) Gibbs free energy of the reaction between barium oxide and water in the formation of barium hydroxide.

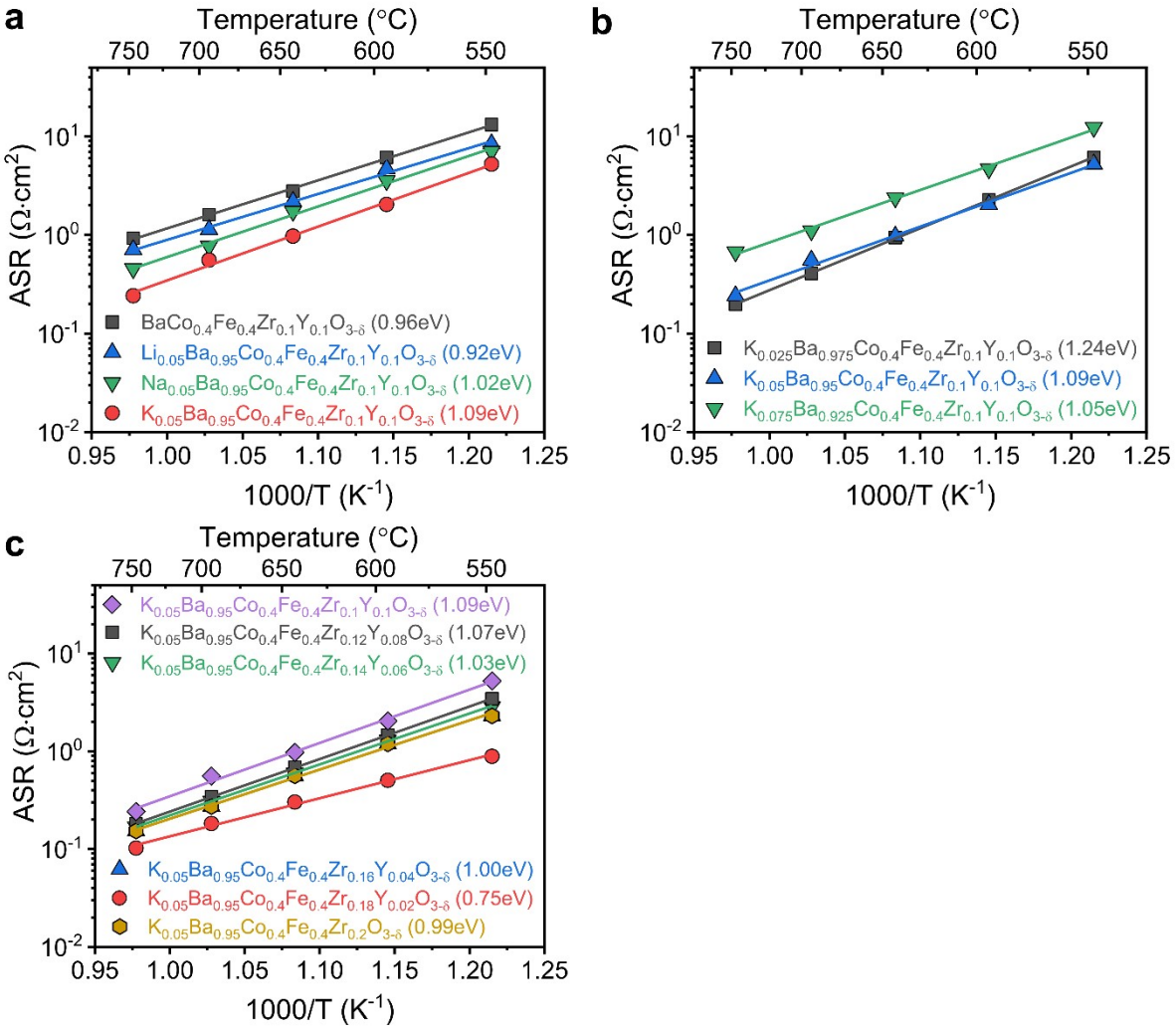

Fig. S11 ASR values of BCFZY and ABCFZY perovskite electrodes on BCZYYb7111 symmetrical cells in wet air (3 vol% H_2O) at 550–750 °C. (a) BCFZY and $A_{0.05}Ba_{0.95}Co_{0.4}Fe_{0.4}Zr_{0.1}Y_{0.1}O_{3-\delta}$ (A = Li, Na, and K) electrodes. (b) $K_xBa_{1-x}Co_{0.4}Fe_{0.4}Zr_{0.1}Y_{0.1}O_{3-\delta}$ (x = 0.025, 0.5, and 0.075) electrodes. (c) $K_{0.05}Ba_{0.95}Co_{0.4}Fe_{0.4}Zr_{0.2-y}Y_yO_{3-\delta}$ (y = 0, 0.02, 0.04, 0.06, 0.08, and 0.1) electrodes.

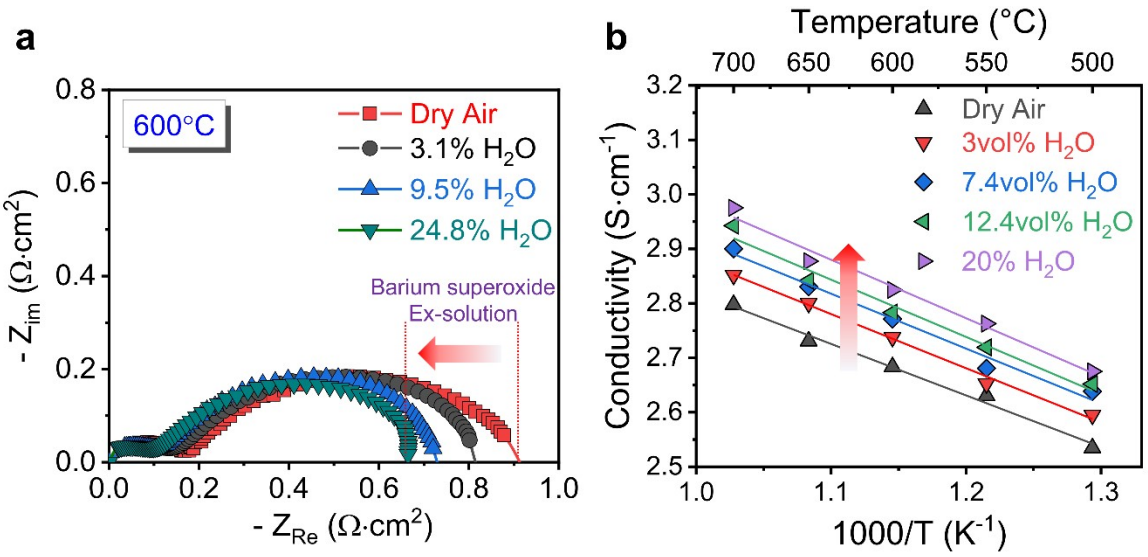

Fig. S12 Electrocatalytic activity measurements of KBCFZY as a function of water vapor concentration in ambient air. (a) Nyquist plots from electrochemical impedance spectroscopy (EIS) measurements of KBCFZY at 600 ℃. (b) KBCFZY electrical conductivity at 500–700 ℃.

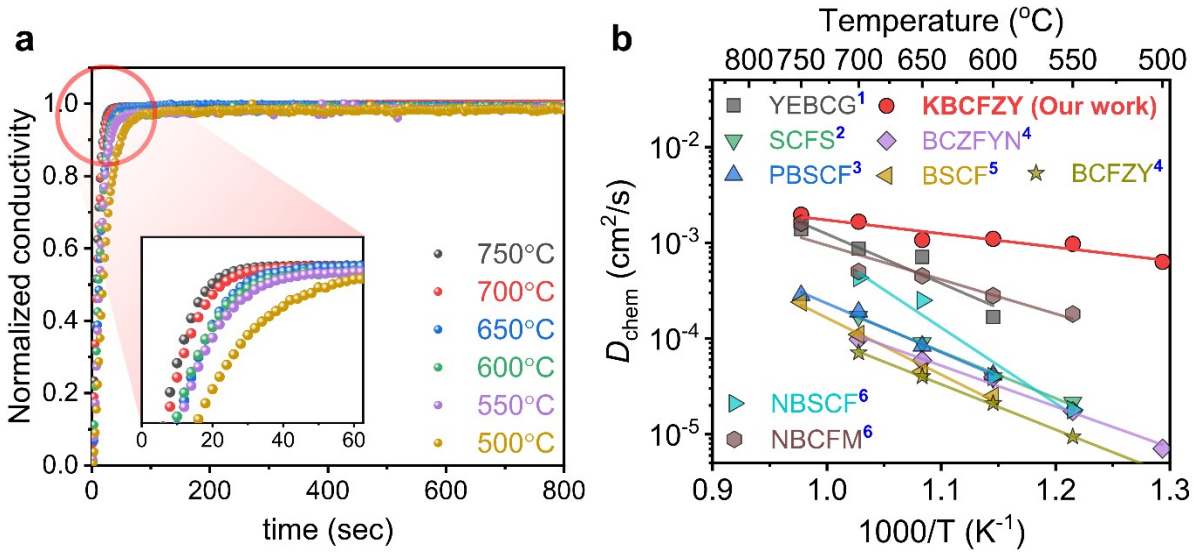

Fig. S13 Electrical conductivity relaxation (ECR) measurements of KBCFZY. (a) ECR profiles of KBCFZY by changing pH_2O at 500–750 ℃. (b) Oxygen-ion bulk diffusion coefficient (D_{chem}) of KBCFZY vs. other oxygen-electrode materials.

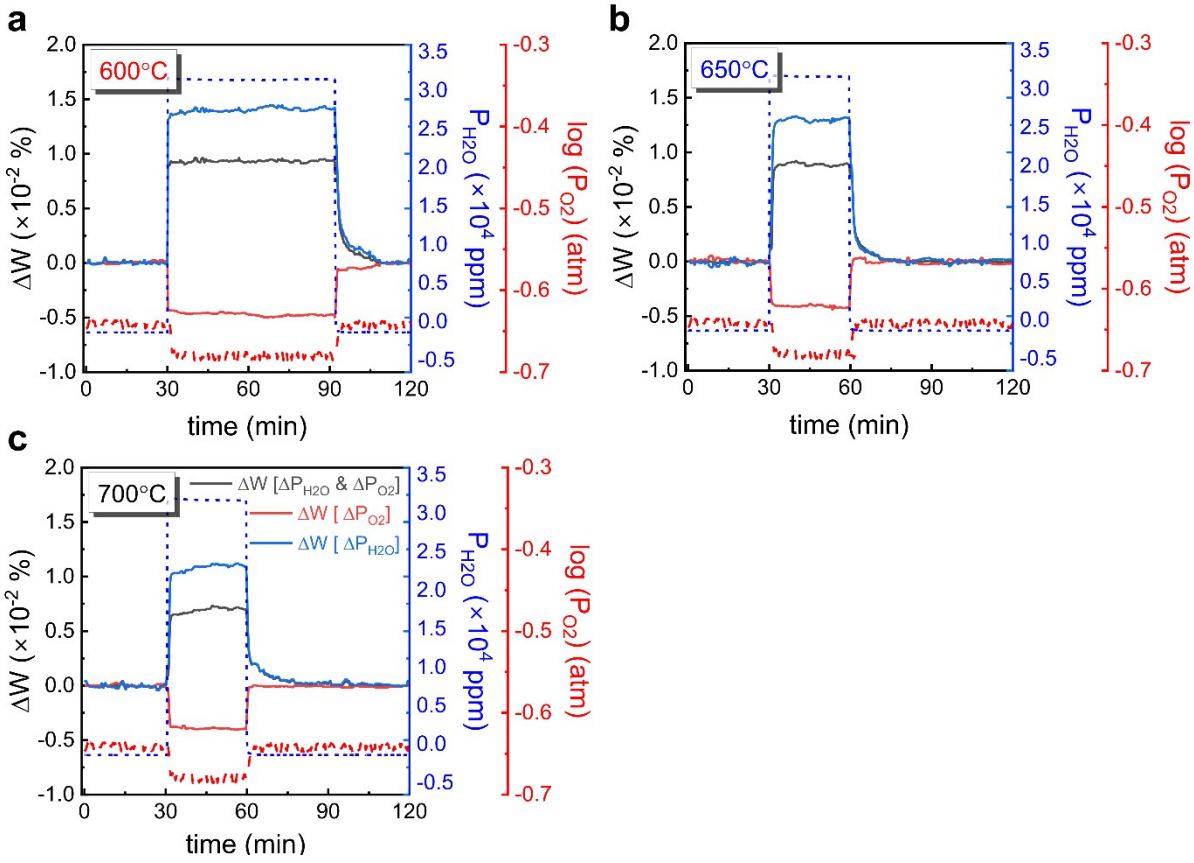

Fig. S14 Weight change (ΔW) according to change of oxygen and water partial pressure by thermal gravimetric analysis. (a) 600 ℃. (b) 650 ℃. (c) 700 ℃.

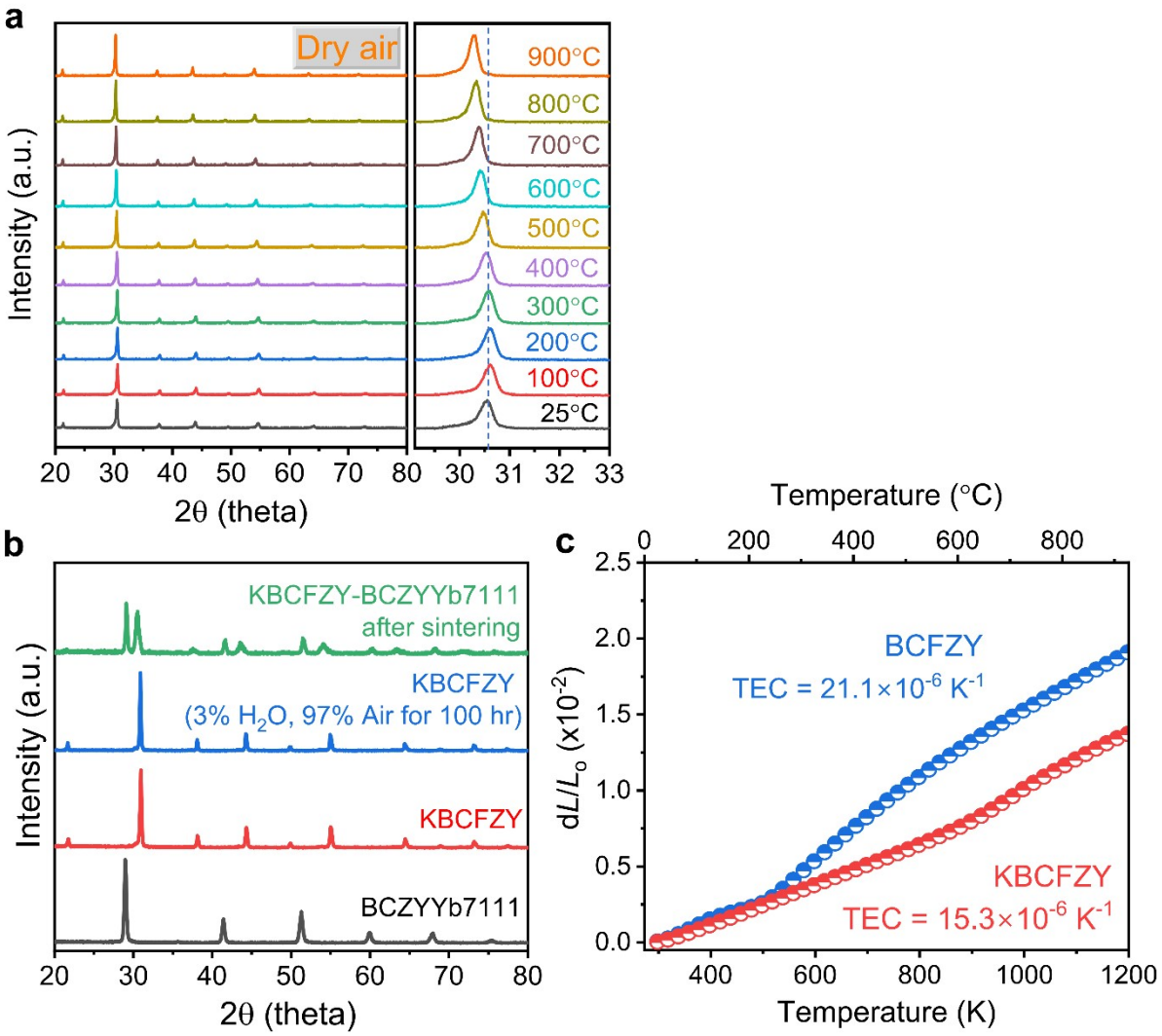

Fig. S15 Crystal structure stability of KBCFZY. (a) In-situ high-temperature XRD patterns of KBCFZY from 25 to 900 ℃. (b) Phase stability analyses from the XRD patterns of KBCFZY powder heat treated in wet (3 vol% H_2O) air for 100 hours at 1100 ℃ and KBCFZY-BCZYYb7111 (50:50) composite powder sintered at 1100 ℃ for 2 hours. (c) Variation of $\Delta L/L_0$ as a function of temperature (25–920 ℃) for BCFZY and KBCFZY.

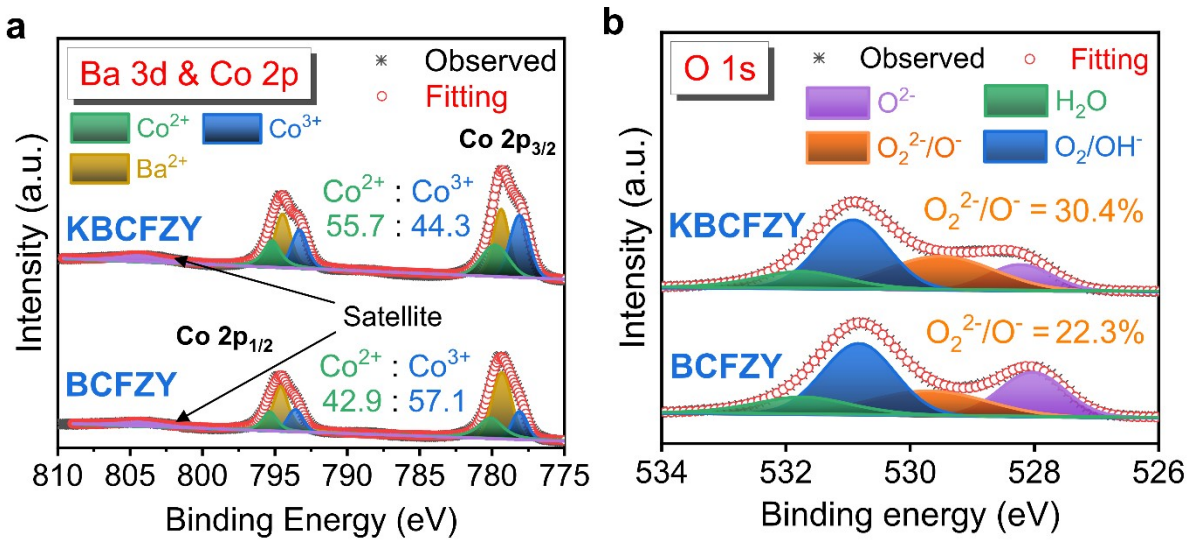

Fig. S16 Electronic structure analysis of BCFZY and KBCFZY by X-ray photoelectron spectroscopy (XPS). (a) Ba 3*d* and Co 2*p* XPS spectra. (b) O 1*s* XPS spectra.

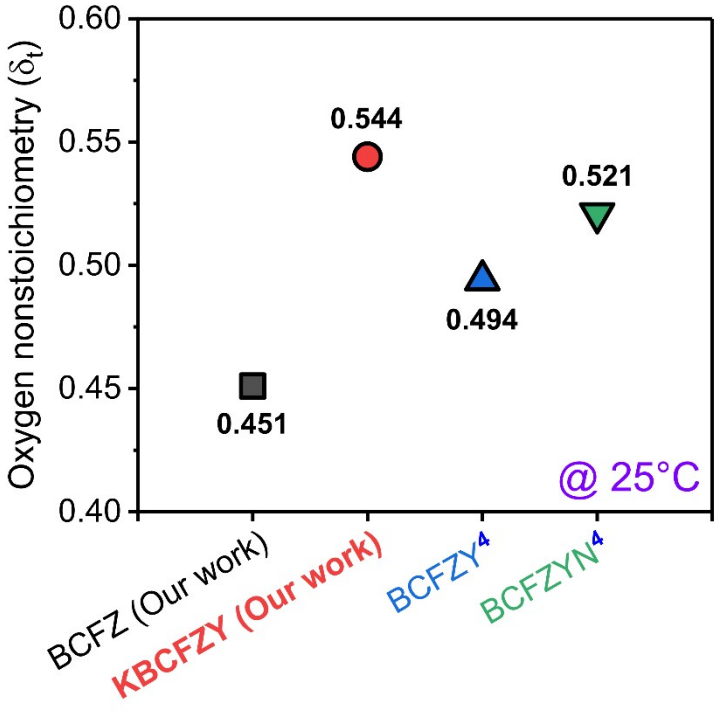

Fig. S17 Comparison of oxygen nonstoichiometry (δ_t) of BCFZY and KBCFZY with other perovskite materials at room temperature.

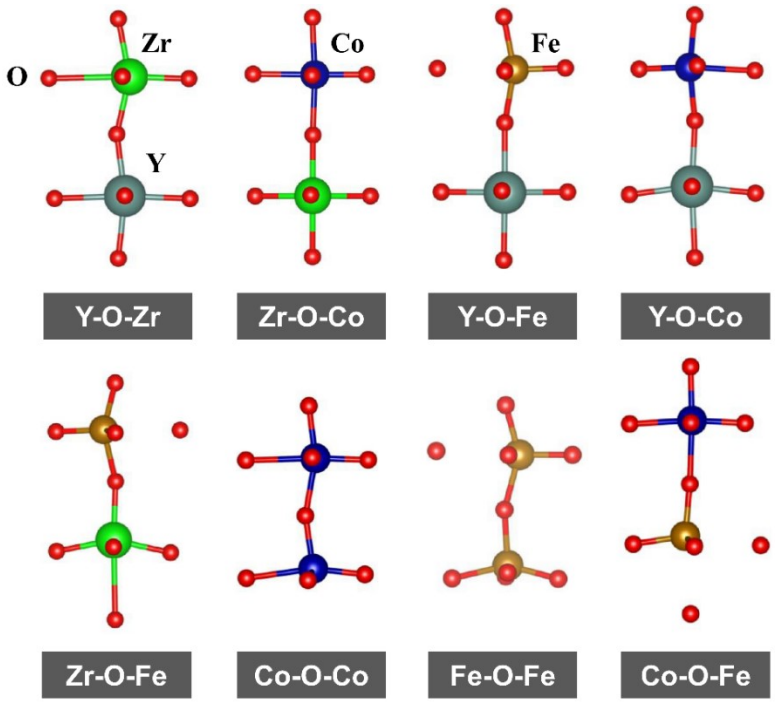

Fig. S18 Eight distinguishable types of metal-oxygen-metal (M-O-M) bond sequences in BCFZY and KBCFZY.

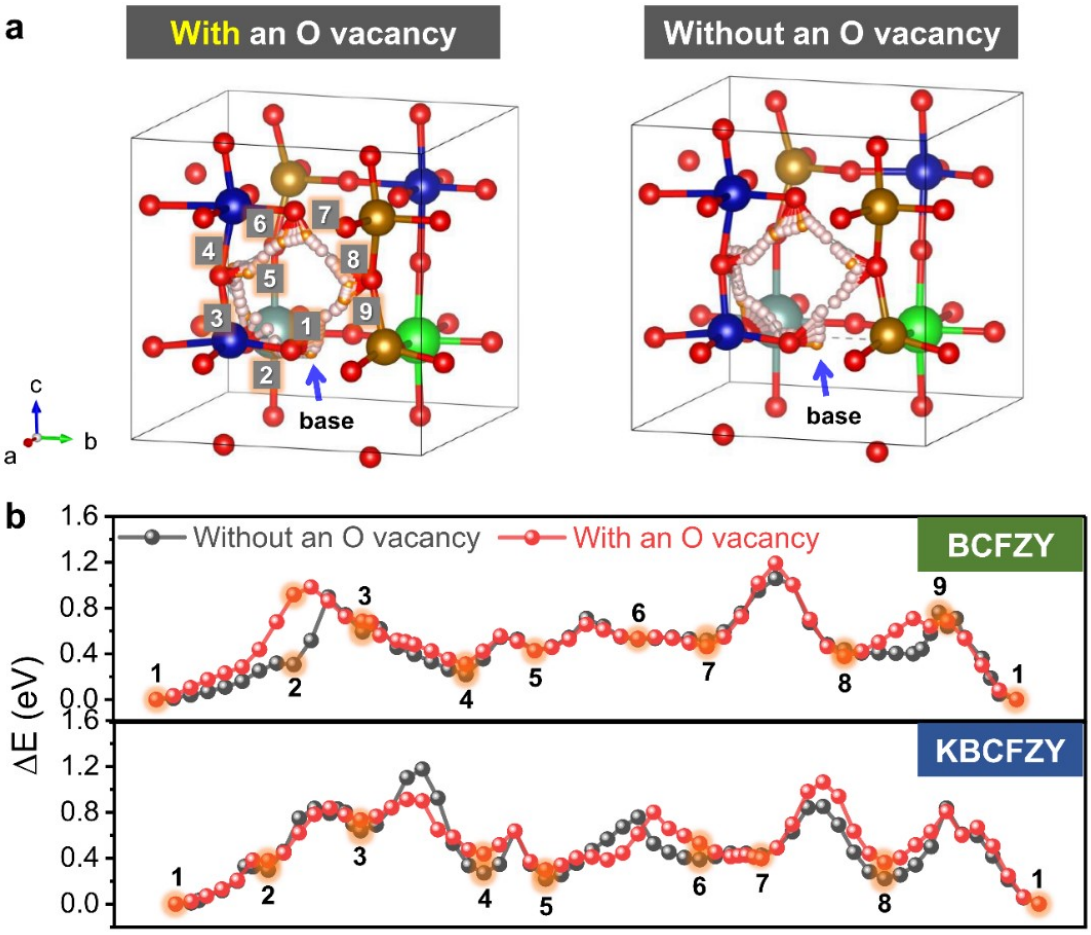

Fig. S19 DFT calculations. (a) Proton migration pathway with and without oxygen vacancy. The stable position of proton is represented by the orange atoms and the most stable position is indicated by the arrow. (b–c) Calculated migration energy with and without oxygen vacancy along the path relative to the energy of the most stable position in BCFZY (b) and KBCFZY (c).

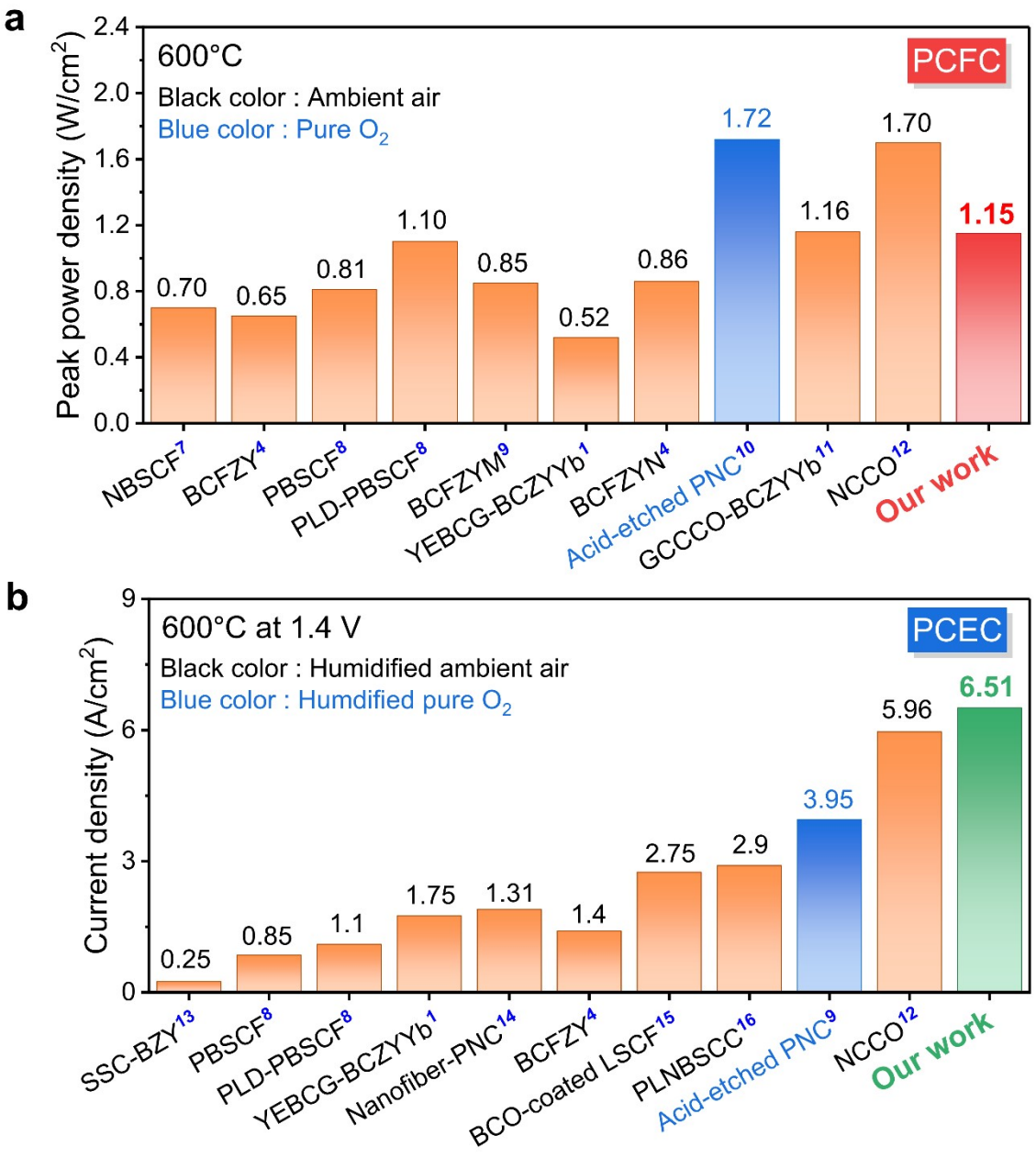

Fig. S20 Performance comparison of KBCFZY vs. other perovskite-based oxygen electrode materials at 600 ℃. (a) Peak power density under PCFC conditions. (b) Current density in PCEC mode at 1.4 V.

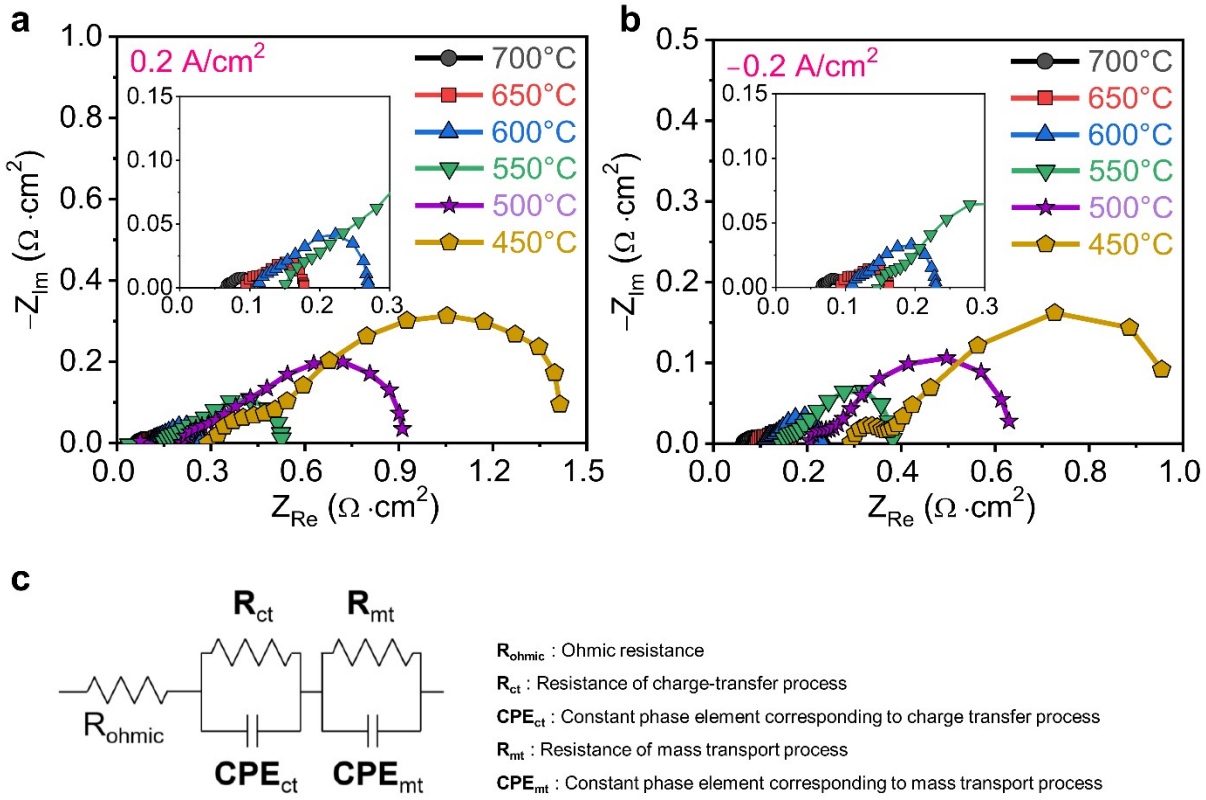

Fig. S21 EIS Nyquist-format spectra of KBCFZY cells under RPCC operation at 450–700 °C. (a) 0.2 A·cm^{-2} in PCFC mode. (b) –0.2 A·cm^{-2} in PCEC mode. (c) Equivalent circuit model of cells.

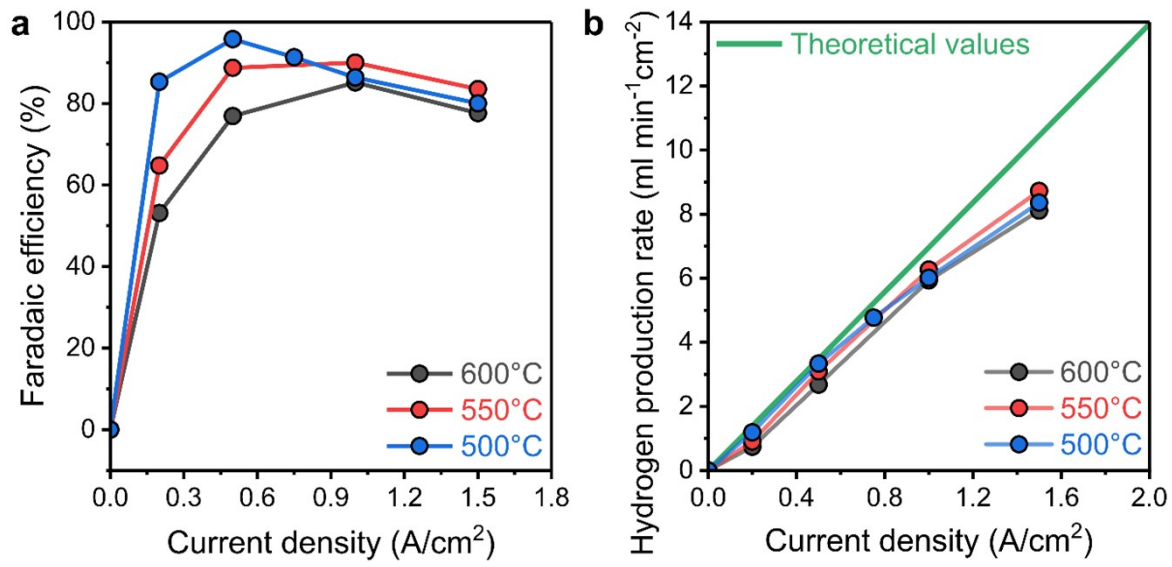

Fig. S22 Hydrogen production of KBCFZY-based cell as a function of current density from 500 to 600 °C. (a) Faradaic efficiency. (b) Hydrogen production rate.

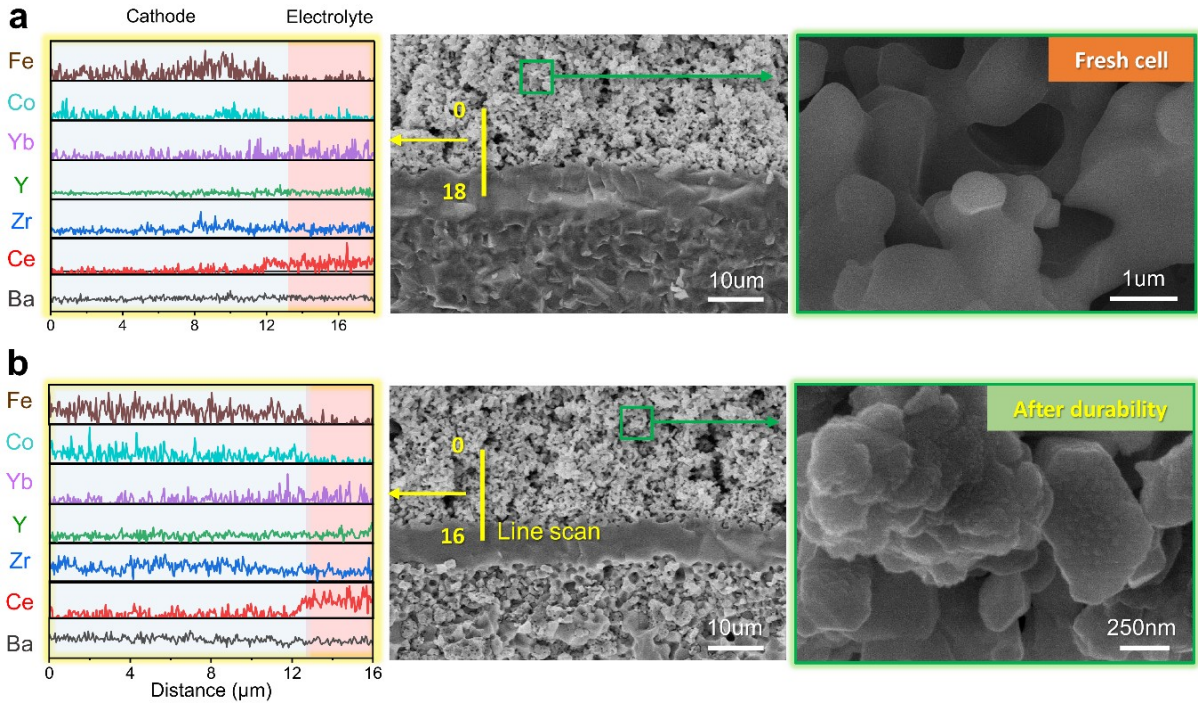

Fig. S23 FE-SEM images and EDX elemental line mapping results of KBCFZY cells before and after durability testing. (a) Cross-section (left) and the air electrode surface (right) of a fresh cell. (b) Cross-section and the air electrode surface of the post-mortem cell after 600 hours of testing at 600 ℃. The K element was not detected due to the low detection limit of SEM/EDX.

References

1. J. S. Shin, H. Park, K. Park, M. Saqib, M. Jo, J. H. Kim, H. T. Lim, M. Kim, J. Kim and J. Y. Park, *J. Mater. Chem. A*, 2021, **9**, 607-621.
2. Y. B. Chen, B. M. Qian and Z. P. Shao, *J. Power Sources*, 2015, **294**, 339-346.
3. Y. Xu, Y. L. Huang, Y. M. Guo, F. Hu, J. M. Xu, W. Zhou, Z. H. Yang, J. Sun, B. B. He and L. Zhao, *Sep. Purif. Technol.*, 2022, **290**, 120844.
4. M. Z. Liang, F. He, C. Zhou, Y. B. Chen, R. Ran, G. M. Yang, W. Zhou and Z. P. Shao, Chem. Eng. J., 2021, **420**, 127717.
5. P. F. Haworth, S. Smart, J. M. Serra and J. C. D. da Costa, *Phys. Chem. Chem. Phys.*, 2012, **14**, 9104-9111.
6. J. I. Lee, K. Y. Park, H. Park, H. Bae, M. Saqib, K. Park, J. S. Shin, M. Jo, J. Kim, S. J. Song, E. D. Wachsman and J. Y. Park, *J. Power Sources*, 2021, **510**, 230409.
7. J. Kim, S. Sengodan, G. Kwon, D. Ding, J. Shin, M. L. Liu and G. Kim, *Chemsuschem*, 2014, **7**, 2811-2815.
8. S. Choi, T. C. Davenport and S. M. Haile, *Energ. Environ. Sci.*, 2019, **12**, 206-215.
9. M. Z. Liang, Y. F. Song, D. L. Liu, L. W. Xu, G. M. Yang, W. Wang, W. Zhou, R. Ran, M. G. Xu and Z. P. Shao, *Appl. Catal. B: Environ.*, 2022, **318**, 121868.
10. W. J. Bian, W. Wu, B. M. Wang, W. Tang, M. Zhou, C. R. Jin, H. P. Ding, W. W. Fan, Y. H. Dong, J. Li and D. Ding, *Nature*, 2022, **604**, 479-485.
11. M. Saqib, I. G. Choi, H. Bae, K. Park, J. S. Shin, Y. D. Kim, J. I. Lee, M. Jo, Y. C. Kim, K. S. Lee, S. J. Song, E. D. Wachsman and J. Y. Park, *Energ. Environ. Sci.*, 2021, **14**, 2472-2484.
12. K. Park, H. Bae, H. K. Kim, I. G. Choi, M. Jo, G. M. Park, M. Asif, A. Bhardwaj, K. S. Lee, Y. C. Kim, S. J. Song, E. D. Wachsman and J. Y. Park, *Adv. Energy Mater.*, 2023,

13, 2202999.

13. F. He, D. Song, R. R. Peng, G. Y. Meng and S. F. Yang, *J. Power Sources*, 2010, **195**, 3359-3364.
14. H. P. Ding, W. Wu, C. Jiang, Y. Ding, W. J. Bian, B. X. Hu, P. Singh, C. J. Orme, L. C. Wang, Y. Y. Zhang and D. Ding, *Nat. Commun.*, 2020, **11**, 1907.
15. Y. C. Zhou, W. L. Zhang, N. Kane, Z. Y. Luo, K. Pei, K. Sasaki, Y. M. Choi, Y. Chen, D. Ding and M. L. Liu, *Adv. Funct. Mater.*, 2021, **31**, 2105386.
16. Z. Q. Liu, Z. J. Tang, Y. F. Song, G. M. Yang, W. R. Qian, M. T. Yang, Y. L. Zhu, R. Ran, W. Wang, W. Zhou and Z. P. Shao, *Nano-Micro Lett.*, 2022, **14**, 217.